Distribution of individual wave overtopping volumes on mound breakwaters

Jorge Molines [a,*], Maria P. Herrera [b], M. Esther Gómez-Martín [c] and Josep R. Medina[d]

[a] Assistant Professor, Dept. of Transportation, *Universitat Politècnica de València*, Camino de Vera s/n, 46022 Valencia, Spain. E-mail: jormollo@upv.es (*corresponding author)

[b] Consultant Engineer at *PROES*, C/ San Germán, 39,28020, Madrid, Spain. E-mail: mherrera@proes.engineering

[c] Assistant Professor, Dept. of Transportation, *Universitat Politècnica de València*, Camino de Vera s/n, 46022 Valencia, Spain. E-mail: mgomar00@upv.es.

[d] Professor, Dept. of Transportation, *Universitat Politècnica de València*, Camino de Vera s/n, 46022 Valencia, Spain. E-mail: jrmedina@upv.es

Keywords: individual wave overtopping volumes, wave overtopping, mound breakwater, Weibull distribution, utility function, number of overtopping waves

Highlights:

- Existing formulas to estimate P_{ow} and maximum individual wave overtopping volume are usually based on tests with large P_{ow}; this study is focused on mound breakwaters subjected to P_{ow} <0.2.
- The new estimators proposed in this study improve the predictions of N_{ow} and maximum individual wave overtopping volumes on conventional mound breakwaters designed under low wave overtopping conditions.
- The mean value of the Weibull distribution fitted to the highest individual wave overtopping volumes may be different from the measured $\bar{V}$.

- New 2-parameter Weibull and Exponential distributions are proposed with unbiased estimations of V_{max}* with rMSE=10.4% and 10.6%, respectively.
- Using the quadratic utility function and the estimated q and N_{ow}, V_{max}* was estimated by the Weibull and Exponential distributions with rMSE=31.6% and 33.3%, respectively.

Abstract

Conventional mound breakwaters are usually designed to withstand low mean wave overtopping discharges and a low proportion of overtopping waves (P_{ow}). Existing formulas to estimate P_{ow} and maximum individual wave overtopping volume are usually based on tests with high P_{ow}; this study is focused on mound breakwaters subjected to $P_{ow} < 0.2$. The performance of the 2-parameter Weibull and Exponential distributions is examined in order to describe individual wave overtopping volumes of mound breakwaters in non-breaking wave conditions. A new methodology is applied to 164 small-scale 2D physical tests to identify the number of overtopping waves, and the corresponding individual wave overtopping volumes. Utility functions are used to consider the relative relevance of the observed data: in this study, a quadratic utility function depending on all the individual wave overtopping volumes and step utility functions with 10%, 30% and 50% of the highest volumes are used to fit the Weibull and Exponential distributions. In this study, a new estimator of P_{ow} is proposed to improve the predictions required to estimate the maximum individual wave overtopping volume. Existing estimators of P_{ow} underpredict the largest values of P_{ow} measured in the physical tests. The parameters fitted to the Weibull and Exponential distributions using the quadratic utility function provide estimations of the dimensionless maximum individual wave overtopping volume with relative mean squared errors rMSE=10.4% and 10.6%, respectively. When CLASH Neural Network-estimated mean overtopping rates are used to predict the maximum individual wave overtopping with the quadratic utility function, the 2-parameter Weibull and Exponential distributions provide rMSE=31.6% and rMSE=33.3%, respectively.

The new estimators proposed in this study improve the predictions of P_{ow} and maximum individual wave overtopping volumes on conventional mound breakwaters designed for low wave overtopping rates.

1. Introduction

Crest elevation of conventional mound breakwaters must ensure wave overtopping discharge below acceptable limits for pedestrians, buildings, operations, etc. There is an extensive literature background related to mean overtopping discharge on mound breakwaters, q(m^3/s/m), with several prediction tools such as those given by EurOtop [1, 2], Van Gent et al. [3] and Molines and Medina [4, 5]. However, the maximum individual wave overtopping volume, V_{max}(m^3/m), may be much higher than the mean individual wave overtopping volume. Franco et al. [6] suggested using the largest individual wave overtopping volume instead of the mean overtopping discharge to evaluate direct hazards, because the largest overtopping volume during a storm will probably produce the most relevant damage to structures, cranes and buildings.

In the literature, individual wave overtopping volumes on coastal structures and defenses are usually fitted using variants of the Weibull distribution initially proposed by Van de Meer and Janssen [7] and Franco et al. [6]. Studies of this kind have been done by Besley [8], Lykke Andersen et al. [9], Victor et al. [10], Zanuttigh et al. [11] and Nørgaard et al. [12]. Most of these studies are based on 2D small-scale tests, but very few of them analyzed in detail the methodology used to identify, in test runs of N_w waves, the number of overtopping waves (N_{ow}) or the proportion of overtopping waves ($P_{ow}=N_{ow}/N_w$) and the individual overtopping volumes (V) given a continuous experimental record of accumulated overtopping volume.

The 2-parameter Weibull distribution given by Eq. [1] and used by Van der Meer and Janssen [7] among others are usually related by means of the measured mean individual wave overtopping volume, $\bar{V}$(m^3/m), so there is only the shape factor as the free parameter to fit the Weibull distribution to the

observed individual wave overtopping volumes. The Weibull scale factor is obtained by forcing the mean value of the Weibull distribution to be equal to $\bar{V}$. Depending on the author, this Weibull free parameter is fitted as a constant value (see Van der Meer and Janssen [7]) or using different explanatory variables such as the relative crown wall crest freeboard and the slope angle (see Victor et al. [10]) or the dimensionless wave overtopping discharges (see Zanuttigh et al. [11]). However, Pan et al. [13] and Gallach [14] pointed out that the two parameters of the Weibull distribution may not be related by the mean individual wave overtopping volume ($\bar{V}$) and hence both parameters of the Weibull distribution should be fitted through the measured individual wave overtopping volumes.

Pan et al. [13] highlighted that the criterion to select the data used to fit the Weibull parameters is not always the same in the literature and there is no justification in the chosen criteria. For instance, Victor et al. [10] and Zanuttigh et al. [11] analyzed smooth impermeable low-crested structures and, conventional and low-crested mound breakwaters, respectively, using the individual overtopping volumes higher than the mean value to better represent the largest volumes; Nørgaard et al. [12] analyzed conventional mound breakwaters in breaking conditions using the 30% highest individual wave overtopping volumes to maintain a sufficient accuracy in the determination of individual overtopping volumes in the model tests with lowest amount of overtopping. Both Hughes et al. [15] and Gallach [14] analyzed smooth impermeable low-crested structures using the 10% highest individual wave overtopping volumes.

$\bar{V}$ depends both on the total overtopped volume and also the number of overtopping waves (N_{ow}), which is not a reliable variable since N_{ow} is difficult to measure in laboratory tests, especially for low individual wave overtopping volumes. In this study, a new methodology is developed to identify low individual wave overtopping volumes and N_{ow} from an accumulated overtopping volume recorded in 2D physical tests. The two parameters of the Weibull and Exponential distributions are fitted using the 10%, 30% and 50% of the highest individual wave overtopping volumes and a quadratic utility function with 100% of

the individual wave overtopping volumes. Special attention is paid to represent the highest individual wave overtopping volume (V_{max}) of each test, because V_{max} is a relevant variable when designing coastal structures.

This paper is structured as follows. Firstly, the literature on individual wave overtopping volumes (V) is reviewed. Secondly, the performance of existing estimators for the number of overtopping waves (N_{ow}) and maximum individual wave overtopping volume (V_{max}) is analyzed. Thirdly, the 2D physical model tests are described. Fourthly, a new methodology to identify individual wave overtopping volumes (V) is developed. Fifthly, the 2-parameter Weibull and Exponential distributions are studied in order to fit the distribution F(V) using four utility functions. Sixthly, the performance of the new estimators of N_{ow} and V_{max} is assessed using measured wave overtopping discharges. Seventhly, the N_{ow} and V_{max} are examined using estimated wave overtopping discharges. Finally, general conclusions are drawn.

2. Literature review on individual wave overtopping volumes

2.1 Weibull distribution to estimate individual wave overtopping volumes

The Weibull distribution was introduced by Van der Meer and Janssen [7] and Franco et al. [6] to describe the distribution of individual wave overtopping volumes for dikes and vertical breakwaters, respectively. Later, the 2-parameter Weibull distribution was considered to study the overtopping volume per wave for many types of coastal structures, such as smooth slopes analyzed by Victor et al. [10] and mound breakwaters analyzed by Nørgaard et al. [12]. The 2-parameter Weibull cumulative distribution function is given by:

$$F(V) = 1 - exp\left[-\left(\frac{V}{a}\right)^{b}\right] \quad (1)$$

where $F(V)$ is the probability of the individual wave overtopping volume per wave being less than or equal to V, a is the scale factor and b is the shape factor. Eq. (1) is commonly rewritten with a= $A\bar{V}$,

where A is the dimensionless scale factor and $\bar{V}$ is the measured mean individual wave overtopping volume.

If the measured data followed a perfect Weibull distribution and all the data were used for the analysis, the mean value of a Weibull distribution, μ, would be given by Eq. (2), equal to the mean individual wave overtopping volume (μ=$\bar{V}$). Under the previous conditions, Eq. (3) would provide the relationship between the parameters A and b, where Γ is the gamma function, $\Gamma(z) = \int_0^\infty t^{z-1}e^{-t}dt$.

$$\mu = A\,\bar{V}\Gamma\left(1+\frac{1}{b}\right) \quad (2)$$

$$A = \frac{1}{\Gamma\left(1+\frac{1}{b}\right)} \quad (3)$$

Van der Meer and Janssen [7] and Franco et al. [6] recommended a shape factor b=0.75 for dikes and vertical breakwaters in non-breaking wave conditions. Based on these two studies, EurOtop [1] recommended a shape factor of b=0.75 for dikes and mound breakwaters whatever the geometrical characteristics. According to Eq. (3), the scale factor corresponding to the shape factor b=0.75 is A=0.84.

Besley [8] conducted a detailed analysis on the individual wave overtopping volumes for vertical walls, sloped structures and composite structures. Besley [8] also reported the tests of Franco [16] who had noticed an influence of the wave steepness on the shape factor (b) for vertical caissons ranging from b=0.66 when s_{0p}=0.02 to b=0.82 when s_{0p} =0.04, where $s_{0p}=2\pi H_{m0}/(gT_p^2)$ is the deep water wave steepness. Franco [16] also indicated that the shape factor (b) for sloped structures was generally higher than that corresponding to vertical structures (b=0.76 if s_{0p}=0.02 and b=0.92 if s_{0p} =0.04). Besley [8] then analyzed sloped structures and provided a shape factor b=0.853 as the average value of all tests. According to Eq. (3), the scale factor corresponding to b=0.853 is A=0.921.

Bruce et al. [17] conducted 2D small-scale tests of wave overtopping on mound breakwaters with different armor units. The authors fitted a shape factor b=0.74 and found that the type of armor and number of layers in the armor had no significant influence on b. Victor et al. [10] conducted 2D small-scale tests to study the distribution of individual wave overtopping volumes on steep, low-crested smooth structures with $0.1 \leq R_c/H_{m0} \leq 1.69$, $0.36 \leq \cot\alpha \leq 2.75$ and $0 \leq P_{ow} \leq 1$ where $P_{ow}=N_{ow}/N_w$ is the proportion of overtopping waves, N_{ow} is the number of overtopping waves and N_w is the total number of incident waves in the test. These authors examined the influence of the slope angle ($\cot\alpha$), relative crest freeboard (R_c/H_{m0}) and wave steepness ($s_{-1,0}$) on the shape factor (b), in which R_c is the crown wall crest freeboard, H_{m0} is the significant wave height and $s_{-1,0}=2\pi H_{m0}/(gT_{-1,0}^2)$. They found a significant influence of $\cot\alpha$ and R_c/H_{m0} on the shape factor (b) but no clear effect of $s_{-1,0}$ on b. Victor et al. [10] proposed Eq. (4) to estimate the shape factor.

$$b = exp\left(-2.0\frac{R_c}{H_{m0}}\right) + 0.56 + 0.15cot\alpha \quad (4)$$

Hughes et al. [15] re-analyzed the tests with smooth slopes reported by Van der Meer and Janssen [7], Hughes and Nadal [18] and Victor et al. [10], using different numbers of data to better determine the shape factor of the Weibull distribution, to fit the largest individual overtopping volumes. Hughes et al. [15] concluded that the best fit to the extreme tail of the individual wave overtopping volume distribution was obtained using only the top 10% of the individual wave overtopping volumes while sacrificing accuracy for the lower volumes. Hughes et al. [15] then proposed Eq. (5) to estimate the shape factor in the range $-2<R_c/H_{m0}<4$ and $0 \leq P_{ow} \leq 1$.

$$b = \left[exp\left(-0.6\frac{R_c}{H_{m0}}\right)\right]^{1.8} + 0.64 \quad (5)$$

Zanuttigh et al. [11] studied the shape factor (b) of smooth-slope and rubble mound breakwater distributions. These authors concluded that rubble mound structures show more scatter in the shape

factor (b) than smooth slopes and suggested relating the shape factor (b) to the dimensionless mean wave overtopping discharges (q) instead of the relative crest freeboard (R_c/H_{m0}), since mean overtopping discharge implicitly includes information such as wave steepness or slope angle. EurOtop [2] recommended the formula proposed by Zanuttigh et al. [11] given by Eq. (6) to estimate the shape factor of conventional and low-crested mound breakwaters with $0<R_c/H_{m0}<2$ and $0.004\leq P_{ow}\leq 1$.

$$b = 0.85 + 1500\left(\frac{q}{gH_{m0}T_{-1,0}}\right)^{1.3} \tag{6}$$

Nørgaard et al. [12] conducted 2D small-scale physical tests with rock armored mound breakwaters with structure slope cotα =1.5 to analyze the distribution of individual wave overtopping volumes in depth-limited wave breaking conditions. Eq. (7) is valid for $0.19\leq H_{m0}/h\leq 0.55$, $0.9\leq R_c/H_{m0}\leq 2.0$, $3.3\leq Ir_m=\cot\alpha/[2\pi H_{m0}/(gT_m^2)]^{0.5}\leq 4.6$, $0.006\leq P_{ow}\leq 0.12$, $7.73\cdot10^{-7}\leq q/(T_m g H_s)\leq 6.19\cdot10^{-5}$ where T_m is the mean period, P_{ow} is the proportion of overtopping waves and q is the mean overtopping discharge. In this study $T_m=T_{01}=m_0/m_1$, in which m_i is the i^{th} spectral moment.

$$b = \begin{cases} 0.75 & \text{for } H_{m0}/H_{\frac{1}{10}} \leq 0.848 \text{ or } H_{m0}/h \leq 0.2 \\ -6.1 + 8.08\, H_{m0}/H_{\frac{1}{10}} & \text{for } H_{m0}/H_{\frac{1}{10}} > 0.848 \text{ and } H_{m0}/h > 0.2 \end{cases} \tag{7}$$

where $H_{m0}=4(m_0)^{1/2}$ is the significant wave height and $H_{1/10}$ is the average of the top 10% highest waves.

Pan et al. [13] examined the influence of the proportion of the largest overtopping events selected before fitting the Weibull parameters over a levee under negative crest freeboard. These authors considered selecting 100% (all overtopping events), the largest 50% and the largest 10%. Pan et al. [13] recommended selecting all individual wave overtopping volumes to fit the Weibull parameters in order to achieve a better performance in the estimation of individual wave overtopping volumes. Pan et al. [13] also proposed estimators for the shape and scale factors depending on the number of data selected

for the analysis (100%, 50% and 10%); the relationship between the shape and scale factors was not the mean individual wave overtopping volume ($\bar{V}$) given by Eqs. (2) and (3). Pan et al. [13] then used the methodology of Hughes and Nadal [18] to identify individual wave overtopping waves for levees with negative crest freeboards under overflow and wave overtopping. The methodology used a script to analyze a wave sensor on the breakwater crest to identify waves as the number of time steps from one wave trough to the following trough. Small waves with periods of less than one second (at prototype scale) were discarded from the analysis since those could be perturbations on the signal. The discarded waves had small volumes in the range 5 to 10% of the average wave volume for the corresponding experiment.

Gallach [14] conducted thousands of 2D small-scale tests on smooth and very steep slopes and vertical structures as well as on very low crest freeboards with $0 \leq P_{ow} \leq 1$. He proposed a shape factor dependent on cotα and R_c/H_{m0} to improve the prediction reported by Victor et al. [10] for the case of zero freeboard. Gallach [14] found that the shape factor (b) is not affected by the roughness of the structure slope. Gallach [14] also noticed that the best fitted scale factor (A) for each test was not the same as the scale factor given by Eq. (3); he provided a 90% confidence band to characterize the uncertainty in the estimation of the scale factor A given a shape factor b.

2.2 Number of overtopping waves and maximum individual wave overtopping volume on mound breakwaters

In order to assess the exceedance probability of a set of values, Makkonen [19] suggested that the Weibull plotting position formula given by Eq. (8) may be used for any underlying continuous function.

$$1 - F(V) = \frac{i}{N_{ow}+1} \tag{8}$$

where F(V) is the probability of observing an individual wave overtopping volume larger than or equal to V; i is the position of the sorted volumes in descending order, where i=1 corresponds to the maximum overtopping volume (V_{max}) and N_{ow} is the number of overtopping events.

Using Eq. (8), Lykke-Andersen et al. [9] expressed the Weibull distribution function as:

$$V_i = A\bar{V}\left[-ln\left(\frac{i}{N_{ow}+1}\right)\right]^{1/b} = A\bar{V}[\ln(N_{ow}+1) - \ln(i)]^{1/b} \qquad \text{i=1 to } N_{ow} \qquad (9)$$

The maximum individual wave overtopping volume (V_{max}) can be estimated by setting i=1 in Eq. (9) which leads to Eq. (10). This equation is similar to Eq. (11) proposed by Besley [8] and EurOtop [1, 2] except that Eq. (10) uses N_{ow}+1 instead of N_{ow}. Lykke-Andersen et al. [9] pointed out that Eq. (11) would predict V_{max}=0 for N_{ow}=1, which is an undesirable inconsistency.

$$V_{max} = A\bar{V}[\ln(N_{ow}+1)]^{1/b} \qquad (10)$$

$$V_{max} = A\bar{V}[\ln(N_{ow})]^{1/b} \qquad (11)$$

The estimated maximum individual wave overtopping volume given by Eq. (10) and Eq. (11) depends on the number of overtopping waves (N_{ow}). Besley [8] proposed Eq. (12) to estimate the number of overtopping waves (N_{ow}) for simple slopes and Eqs. (13) to consider more complex sloped structures which include berms or return walls.

$$P_{ow} = exp\left(-K1\left(\frac{R_c}{T_m\sqrt{gH_s}}\frac{1}{\gamma_f}\right)^2\right) \qquad (12)$$

$$P_{ow} = 55.4Q^{*0.634} \qquad for\ 0 < Q^* < 8\cdot 10^{-4} \qquad (13a)$$

$$P_{ow} = 2.50Q^{*0.199} \qquad for\ 8\cdot 10^{-4} \le Q^* < 10^{-2} \qquad (13b)$$

$$P_{ow} = 1 \qquad for\ Q^* \ge 10^{-2} \qquad (13c)$$

where P_{ow} is the proportion of overtopping waves, g is the gravity acceleration, H_s is the significant wave height, T_m is the mean period, $Q_* = q/(T_m g H_s)$ and q is the dimensionless and dimensional mean wave overtopping discharge. In this study, $T_m=T_{01}=m_0/m_1$, and K1=37.8 and 63.8 for structure slope cotα =2 and 1, respectively.

Nørgaard et al. [12] proposed Eqs. (14) to estimate N_{ow} based on estimations given by Eqs. (13), N_{ow}[Eq.(13)].

$$N_{ow} = K2N_{ow}[Eq.(13)] \tag{14a}$$

$$K2 = \begin{cases} 1 & \text{for } H_{m0}/H_{\frac{1}{10}} \leq 0.848 \text{ or } H_{m0}/h \leq 0.2 \\ -6.65 + 9.02\, H_{m0}/H_{\frac{1}{10}} & \text{for } H_{m0}/H_{\frac{1}{10}} > 0.848 \text{ and } H_{m0}/h > 0.2 \end{cases} \tag{14b}$$

To estimate the number of overtopping waves, EurOtop [1, 2] proposed Eqs. (15) and (16) for breakwaters with and without a permeable crest berm ($A_c>R_c$), respectively.

$$P_{ow} = exp\left(-\left(\frac{A_c D_n}{0.19 H_{m0}^2}\right)^{1.4}\right) \tag{15}$$

$$P_{ow} = exp\left(-\left(\sqrt{-ln0.02}\,\frac{R_c}{R_{u2\%}}\right)^2\right) \tag{16}$$

where $R_{u2\%}$ is the run-up exceeded by 2% of the waves, A_c is the armor crest freeboard and D_n is the nominal diameter of the armor unit. EurOtop [1, 2] also proposed Eqs. (17) to estimate the $R_{u2\%}$.

$$\frac{R_{u2\%}}{H_{m0}} = 1.65\gamma_f\gamma_\beta Ir_{-1,0} \tag{17a}$$

$$\text{With } \max\left(\frac{R_{u2\%}}{H_{m0}}\right) = \min\left(1.00\gamma_{fsurging}\gamma_\beta\left[4.00 - \frac{1.50}{\sqrt{Ir_{-1,0}}}\right], 2.0\right) \tag{17b}$$

where $\gamma_{fsurging} = \gamma_{f+(Ir_{-1,0}-1.8)(1-\gamma_f)/8.2}$, γ_β is the reduction factor to account for the oblique wave attack, and $Ir_{0,-1}= \tan\alpha/[2\pi H_{m0}/(gT_{-1,0}^2)]^{0.5}$.

Victor et al. [10] and Gallach [14] suggested different estimators to calculate P_{ow} for low-crested structures depending on the slope angle and the dimensionless crest freeboard with $0 \leq P_{ow} \leq 1$. Hughes and Nadal [18] investigated the probability distribution of individual overtopping volumes for dikes subjected to wave overtopping and storm surge overflow with $-2 < R_c/H_{m0} < 0$ and $P_{ow}=1$.

3. Experimental data

Smolka et al. [20] carried out small-scale tests in the wave flume of the Laboratory of Ports and Coasts at the *Universitat Politècnica de València* (LPC-UPV). The LPC-UPV wave flume (1.2x1.2x30m) has a piston wave-maker with AWACS active wave absorption system.

The cross-section shown in Figure 1 corresponds to cube- and Cubipod-armored mound breakwaters in non-breaking wave conditions with a crown wall and no toe berm; the armor slope was $\cot\alpha=1.5$, and the armor crest berm width was G_c[Cubipod armors]$=3D_n$ and G_c[Cube armor]$=2D_n$. Two water depths were tested in the model zone, h(m)=0.50 and 0.55. Two crown-walls were tested with heights of 0.20 and 0.26 m, $0.203 \leq R_c(m) \leq 0.263$. The model was designed to avoid significant damage to the armor layer. Three armor layers with concrete armor units, $\rho_{Cubipod}(kg/cm^3)=2.29$ and $\rho_{Cube}(kg/cm^3)=2.23$, were tested: (1) conventional double-layer cube armor with $D_n(cm)=6.00$ and $\phi=1.26$, (2) single- and (3) double-layer Cubipod armor with $D_n(cm)=3.82$ and $\phi=0.61$ and 1.18, respectively (see Figure 1), where

ϕ is the packing density.

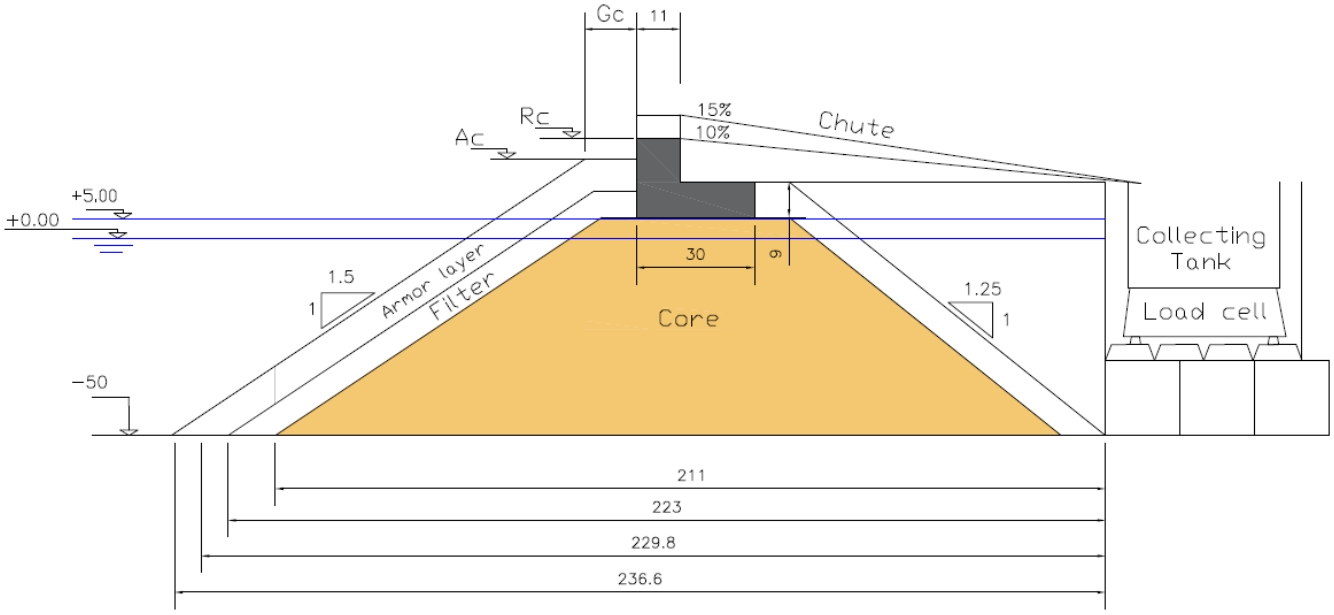

Figure 1. Cross-section tested by Smolka et al. [20]. Dimensions in centimeters.

During the tests, wave overtopping, crown wall stability (see Molines et al. [21]) and armor layer damage were analyzed. Eight capacitance wave gauges sampled at 20 Hz were used in these experiments to separate incident and reflected waves (Figure 2); one group of four wave gauges was placed in front of the wave maker, h(m)=0.75 and 0.80, and the other group of four wave gauges was placed near the model, h(m)=0.50 and 0.55, both groups on horizontal bottoms. A 4% bottom slope transition reduced the water depth at the model area, Δh(m)=0.25, from that of the wave generation zone. An isolated 0.20 m-width chute collected the overtopping discharge and the accumulated volume was obtained by weighing the collecting tank at frequency 5Hz. The sensitivity of the overtopping measurement system was 0.01 kg; for tests with high mean overtopping discharge, pumping operations were necessary because of the limited volume of the collecting tank. Pumping operations were manually conducted during the tests by a trained operator when no overtopping was expected. Figures 5a and 5b show a gross signal in the scale including pumping operations and the corrected scale signal, respectively.

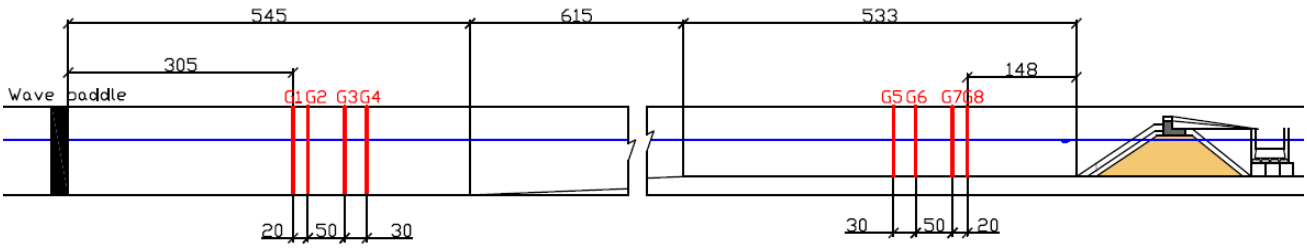

Figure 2. Longitudinal cross-section of the wave flume of the LPC-UPV. Dimensions in centimeters.

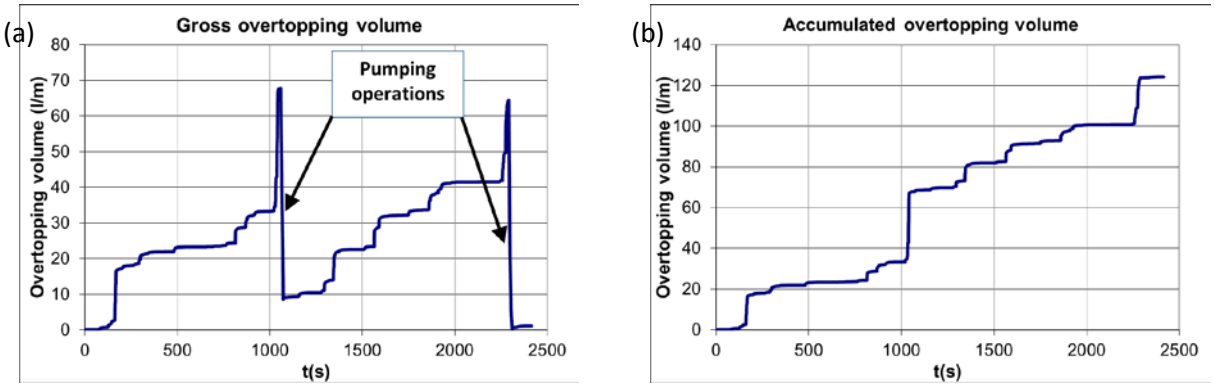

Figure 3. Gross record of accumulated overtopping volume: (a) with pumping operations and (b) eliminating pumped volume.

The model was tested with regular and irregular waves, increasing the incident wave height while maintaining approximately constant the Iribarren number $Ir_m=\tan\alpha/(H_{m0}/L_m)^{0.5}$=2.0, 2.5, 3.0, 3.5 and 4.0 until armor damage or massive overtopping occurred, where L_m is the local mean wavelength at the toe. 1000 irregular waves were generated following the JONSWAP spectrum with γ=3.3. The LASA-V method (Figueres and Medina [22]) was applied to separate the incident and reflected waves. To this end, wave gauges were separated in the range $L_m/4$ to $L_m/8$ in the generation and model areas.

In all, 164 irregular tests of double-layer randomly-placed cube armor and single- and double-layer Cubipod armors were used in the present study; the characteristics are summarized in Table 1.

Armor type	No. tests	H_s (m)	T_{01} (s)	R_c (m)	A_c (m)	G_c (m)	cot α	h (m)

Cube (2L)	39	0.078-0.162	0.947-2.330	0.203-0.263	0.19-0.240	0.120	1.50	0.500-0.550
Cubipod (2L)	66	0.055-0.149	0.871-2.366	0.203-0.263	0.150-0.200	0.120	1.50	0.500-0.550
Cubipod (1L)	59	0.064-0.152	0.881-2.351	0.203-0.263	0.110-0.160	0.120	1.50	0.500-0.550

Table 1. Dimensions and wave conditions of the tests described by Smolka et al. [20].

4. Methodology to identify individual wave overtopping volumes

Continuous overtopping measurements of accumulated overtopping volume are usually recorded during the 2D small-scale tests using (1) wave gauges inside the collecting tank to measure variations in water level or (2) load cells below the collecting tank to weigh variations in mass. On the one hand, measurements with wave gauges require collecting tank sections small enough to be accurate since measurements are affected by oscillations during overtopping events. On the other hand, weigh measurement with load cells may be affected by an added apparent mass generated by the largest overtopping discharges. A sound identification method of the individual wave overtopping volumes from a recorded time series of accumulated overtopping volume is crucial for repeatability and to avoid errors when analyzing the number of overtopping waves and the individual volume of each overtopping event. A variety of methods based on relevant subjective elements is described in the literature.

Besley [8] reported a methodology based on two steps. First, wave gauges were placed at the structure crest to identify the individual wave overtopping events. Second, if load cells were used, the difference in water volume in the collecting tank between two successive overtopping events was the individual wave overtopping volume (considering a time delay between the detected overtopping wave on the crest and the increase in the accumulated overtopping volume in the collecting tank). If water level gauges were used, Besley [8] proposed taking the average of the level readings over the last few seconds

before the arrival of the next overtopping event as the baseline to evaluate individual wave overtopping volumes. Nørgaard et al. [12] used water level gauges in a small collecting tank with an algorithm to identify rapid changes in the volume of water therein and compared the results of the algorithm with visual inspections of the time series of the accumulated overtopping volume after each test. Studies such as those by Victor et al. [10] or Zanuttigh et al. [11] did not describe any specific methodology to identify the number of overtopping waves or to measure the individual wave overtopping volumes.

The methodology used to determine the number of overtopping waves (N_{ow}) affects the estimation of $\bar{V}$ and V_{max}. When a low individual wave overtopping event occurs, it is difficult to separate it from water falling in the collecting tank after a large overtopping event or noise generated by dynamic loads. Conventional mound breakwaters are usually designed to allow low overtopping discharges with very few overtopping waves; a robust measurement of N_{ow} is relevant in this case. In this study, a new methodology is developed to measure the number of overtopping waves and the individual wave overtopping volumes using the continuous record of the accumulated overtopping volume in the collecting tank. In this study, a load cell below the collecting tank was used to weigh variations in mass. The methodology is described in ten steps which are detailed below.

Step 1

The mass record of the load cell, W(kg), is transformed into volume, V_{o1}(l). Only tests with W(kg)>0.01 (related to the load cell sensitivity) are considered in the analysis. In this study, the sampling frequency is 5Hz.

Step 2

The accumulated overtopping volume, V_{o2}(l), is obtained from V_{o1}(l) taking into account the manual pumping operations; V_{o2}(l) is a non-decreasing corrected record, $V_{o2}(t_i) \geq V_{o2}(t_{i-1})$. Later, the accumulated volume, V_{o2}(l), is corrected to consider the width of the chute, C(m)=0.2, $V_{o3}(t_i) = V_{o2}(t_i)/C$.

Step 3

A continuous record of the derivative of the volume, q_1(l/s/m), is obtained from the volume corrected accumulated overtopping V_{o3}(l/m) as:

$$q_1(t_i) = \frac{V_{o3}\left(t_i + \frac{T_{01}}{2}\right) - V_{o3}(t_i)}{\frac{T_{01}}{2}} \qquad i=1\ldots\ldots L_1 \text{ with } L_1=\max(i)-\text{round}(5T_{01}/2) \qquad (18)$$

Eq. (18) was calculated for intervals $T_{01}/2$ because overtopping events discharge water during the crest phase of the wave, which roughly corresponds to half the mean wave period (T_{01}). Time series of q_1(l/s/m) have local peak values near the starting points of possible overtopping events.

Step 4

The derivative of the volume q_1(l/s/m) was filtered using a triangular moving average function given by:

$$q_2(t_j) = 0.25q_1(t_{j-1}) + 0.5q_1(t_j) + 0.25q_1(t_{j+1}) \qquad j=2\ldots\ldots L_2\text{-}1 \text{ with } L_2=\max(j) \qquad (19)$$

Eq. (19) eliminates frequency noise higher than 3Hz in the derivative of the volume, q_1(l/s/m), due to dynamic loads generated by water falling into the collecting tank. The time of the local peaks of q_2(l/s/m) roughly corresponds to the beginning of possible overtopping events (Figure 4). The number of local peaks of q_2(l/s/m) is denoted as Np1.

Step 5

The individual wave overtopping volumes, V_1(l/m), are calculated using Eq. (20) and V_{o3}(l) from Step 2:

$$V_1(t_k) = V_{o3}(t_{k+1}) - V_{o3}(t_k) \qquad \text{k=1……Np1} \qquad (20)$$

where t_k is the time when q_2(l/s/m), given in Step 4, shows a local peak and a possible overtopping event. The higher values of V_1(l/m) always correspond to real overtopping events, but not all the small values of V_1(l/m) correspond to a real overtopping event. Small values of V_1(l/m) may be generated by water continuously falling into the collecting tank after a large overtopping event or generated by a small real wave overtopping event (see Figure 4).

Step 6

During the tests, it was observed that individual wave overtopping volumes higher than 0.25 l/m always corresponded to real overtopping waves. Therefore, the individual wave overtopping volumes, V_1(l/m), were compared with a low threshold V_T(l/m)=0.25. If $V_1(t_k) > V_T$, then $V_1(t_k)$ was considered a real overtopping event. Volumes under the threshold level $V_1(t_k) < V_T$ may correspond to water falling in the collecting tank after a large overtopping event or a small real overtopping event. In the next steps, t_k identifies both the real and possible overtopping events.

Considering a scale 1/50, the value of the threshold V_T at prototype scale is $0.25x(50^3/50)$=625 l/m, near the acceptable limits of 600 l/m for pedestrians suggested by EurOtop [2].

Step 7

When $V_1(t_k) < V_T$, two scenarios may occur: (1) small overtopping events with local peaks of $q_2(t_k) = q_2(t_{k+1}) = q_2(t_{k+2}) = \ldots$ with an increasing time delay between peaks, and (2) small overtopping events with a local peak of $q_2(t_k)$, higher than the surrounding local peaks. Both cases are analyzed separately:

(1) When a small $V_1(t_k)$ with local peaks of $q_2(t_k) = q_2(t_{k+1}) = q_2(t_{k+2}) = \ldots$ is caused by water falling after a large overtopping event, $q_2(t_k)$, $q_2(t_{k+1})$, $q_2(t_{k+2})$,… show an increasing time delay ($t_{k+1} - t_k \leq t_{k+2} - t_{k+1}$) and the

time delay between peaks can be used to identify the starting time of a real overtopping event. The time position t_k(s) may be a real overtopping event if a decreasing time delay is observed between two local peaks.

(2) There is also small real overtopping event at t_k(s) if a local peak value of $q_2(t_k)$ is higher than the surrounding local peaks, $q_2(t_k) > q_2(t_{k-1})$ and $q_2(t_k) > q_2(t_{k+1})$.

Step 8

The individual wave overtopping volumes, V_2(l/m), are calculated using Eq. (21):

$$V_2(t_m) = V_{o3}(t_{m+1}) - V_{o3}(t_m) \qquad \text{m=1……Np2} \qquad (21)$$

where t_m(s) and Np2 are the time positions and the number of real overtopping events obtained after Steps 6 and 7.

Step 9

Small real overtopping events from Step 7 were added to the large overtopping events detected in Step 6. Thus, the time delay between all real overtopping events is analyzed in Step 9. V_2(l/m) is sorted in descending order, with $V_2(t_1)$=max(V_2 (t_m); t_m=1 to Np2). Starting with $V_2(t_1)$, if an overtopping event was closer than $0.8T_{01}$, $|t_m-t_1|<0.8T_{01}$, the overtopping event at t_m(s) was eliminated, since it is not possible to have two waves closer than T_{01}.

Step 10

The individual wave overtopping volumes, V(l/m), are calculated using Eq. (22):

$$V(t_n) = V_{o3}(t_{n+1}) - V_{o3}(t_n) \qquad \text{n=1……N}_{ow} \qquad (22)$$

where t_n(s) and N_{ow} are the time positions and the number of overtopping events obtained after Step 9.

The total V_{03} (l/m) obtained after the volume detection provided $r^2 \approx 1$ when compared to the total measured V_{03} (l/m). Figure 4c compares the measured V_{03} (l/m) and the reconstructed V_{03} (l/m) for Test#41 following the methodology described herein.

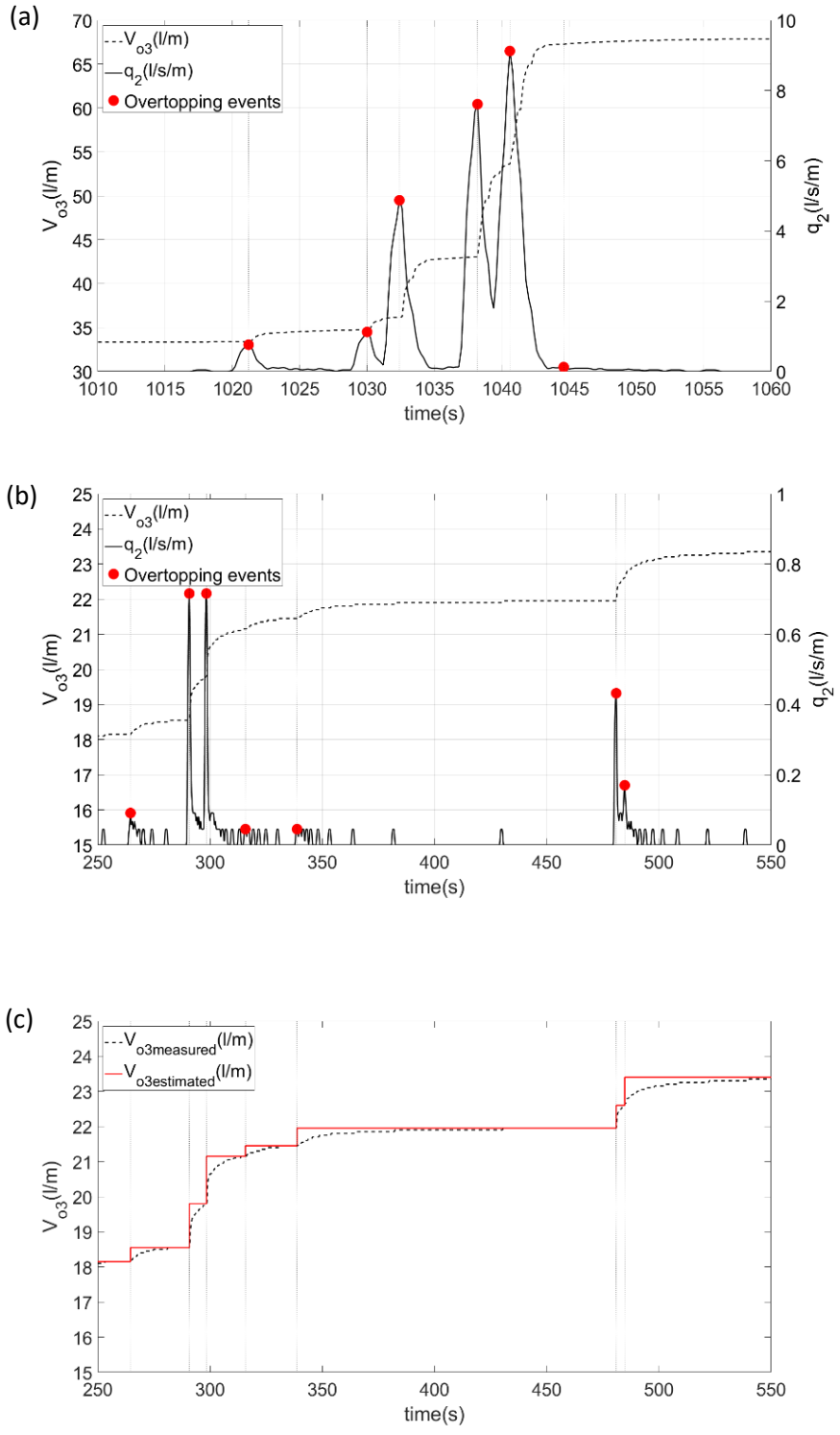

Figure 4. Time series of corrected accumulated overtopping volume (V_{o3}) and filtered derivative of the volume (q_2) of Test #41 with P_{ow}=0.076, H_{m0}(m)=0.12 and T_p(s)=2.53: a) interval between 1010 s and 1060 s, b) interval between 250 s and 550 s and c) comparison of $V_{o3measured}$ (l/m) and $V_{o3estimated}$ (l/m) reconstructed following the methodology described in Section 5 between 250 s and 550 s.

5. Analysis of data

5.1 Weibull parameter fittings

Given Eq. (1) with a= $A\bar{V}$, the Weibull plot can be generated by taking logarithms on both sides twice:

$$ln(-ln(1-F(V))) = b(ln(V/\bar{V}) - ln(A)) \quad (23)$$

Thus, the Weibull plot can be represented considering $ln(-ln(1-F(V)))$ in the y-axis and $ln(V/\bar{V})$ in the x-axis. When the data are represented in a Weibull plot, the slope and the intercept of the fitted line allow to estimate the shape and scale factors of the Weibull distribution, respectively.

The literature review showed that the shape factor (b) of the Weibull distribution is usually fitted to the data as the slope of the straight line in the Weibull plot, and the scale factor (A) is calculated using Eq. (3). Authors such as Pan et al. [13] or Gallach [14] pointed out that the fitted scale factor (A) cannot be the same as that obtained by Eq. (3), since substantial differences were observed between measured and estimated scale factors.

The Weibull distribution is usually fitted to the highest individual wave overtopping volumes (V), for instance, 10% or 30% of the highest V. However, if Eq.(2) is used to estimate the scale factor (A), the low individual wave overtopping volumes and the number of overtopping waves (N_{ow}) are relevant to estimate A because $\bar{V} = V_{total}/N_{ow}$. N_{ow} and $\bar{V}$ are not variables easily measured in laboratory tests (see Section 5); N_{ow} and $\bar{V}$ are subjected to a high uncertainty and are affected by low V, which are not relevant for most practical applications. In order to provide a good representation of the distribution of the highest individual wave overtopping volumes, both the shape and scale factor (b and A) must be obtained from the Weibull plot, although the mean value μ given by Eq. (2) may be different from measured $\bar{V}$.

L1 represented in Figure 5 corresponds to the Weibull distribution with A and b parameters fitted to the highest 10% of individual wave overtopping volumes (Test #32 with H_{m0}(cm)=12.5 and T_p(s)=1.69). If the condition $\mu=\bar{V}$ is imposed and Eq. (3) is used to estimate the scale factor (A), L1 changes to L2; Figure 5 illustrates how the intercept of the straight line L2 changes from I1 to I2, decreasing the goodness of fit to the highest individual wave overtopping volumes. The slope of the lines L1 and L2 is the same, but L2 does not describe the highest individual wave overtopping volumes as well as L1.

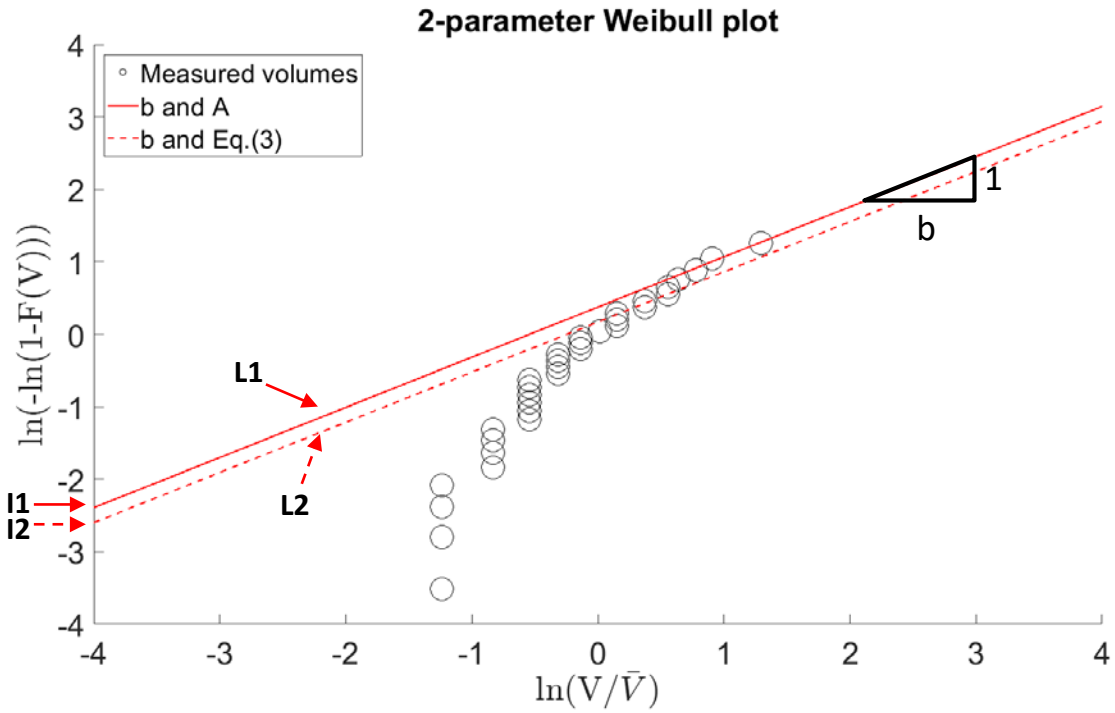

Figure 5. Measured and estimated individual wave overtopping volumes of Test #32 with P_{ow}=0.033.

The shape and scale factors in Figure 5 depend on the number of data used to fit the Weibull distribution. As seen in the literature review, there is no consensus as to the number of data to be selected when fitting the parameters of the probability distributions of individual wave overtopping volumes. 100%, 30% and 10% of the highest individual wave overtopping volumes have been used by different authors.

In this study, the concept of utility function is used in the next section to better describe the data used to fit the shape and scale factors, b and A.

5.2 Utility function

Utility functions, f(u), are used to consider the relative relevance of the observed data; the weights used to fit a mathematical model to a set of data depends on the f(u). Considering the utility function concept, only step utility functions are considered in the literature (see Figure 6a) with a different cut-off threshold $0 \leq VP < V_{max}$ (where P is the percentage of V_i above the threshold, $V_i > VP$). However, it is not easy to justify why individual volumes slightly lower than VP are discarded from the analysis while individual volumes slightly higher than VP are used; a discontinuous utility function (e.g. step function) is not consistent. On the contrary, a continuous and monotonically increasing utility function is recommended for a problem in which the higher the V_i, the higher the relevance for practical applications. Nevertheless, the selection of the best utility function depends on the specific application which is not always known in advance. A continuous and monotonically increasing f(u) avoids the inconsistency in the step utility function but not the subjectivity in selecting the utility function.

In this study, a quadratic utility function depending on the individual wave overtopping volume is used to fit the parameters of the probability functions. The quadratic utility function uses all measured individual wave overtopping volumes (V_i), but the larger V_i have a higher relative weight in the fitting process.

In this section, the step utility functions with VP=V10, V30 and V50 and the quadratic utility function are considered. Using a 2-parameter Weibull plot, the Weibull distribution was fitted by weighted least squares method; this is represented by a straight line. When the step utility functions were used, each V_i was represented by one point in the Weibull plot; when the quadratic utility function was used, each

V_i was represented by a number of virtual points proportional to its weight. Figure 6a illustrates the step utility function, f(u)=0 if $0 \le V_i < VP$, and f(u)=1 if $VP \le V_i \le V_{max}$, and Figure 6b illustrates the quadratic utility function, $f(u)=(V/V_{max})^2$, $0 \le V_i \le V_{max}$. In Figure 6, the x-axis represents the sorted individual wave overtopping volumes (V_i) in ascending order.

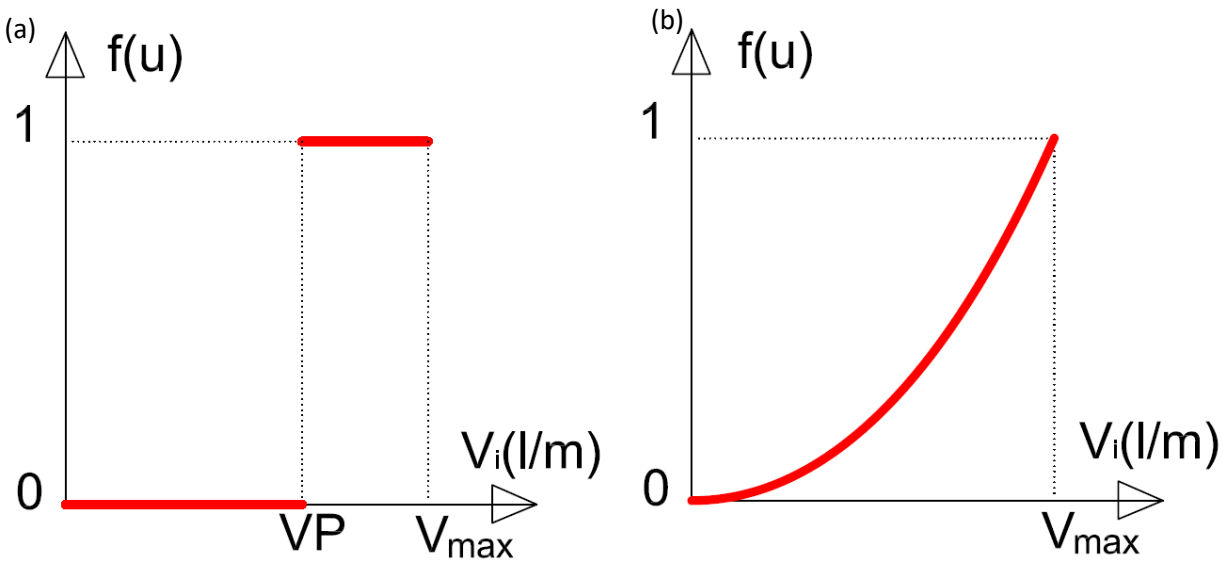

Figure 6. Utility function: (a) step function, and (b) quadratic function.

Figure 7 illustrates the difference in the shape and scale factors (b and A) of the best-fitting of the Weibull distribution of measurements corresponding to Test #32, depending on the utility function.

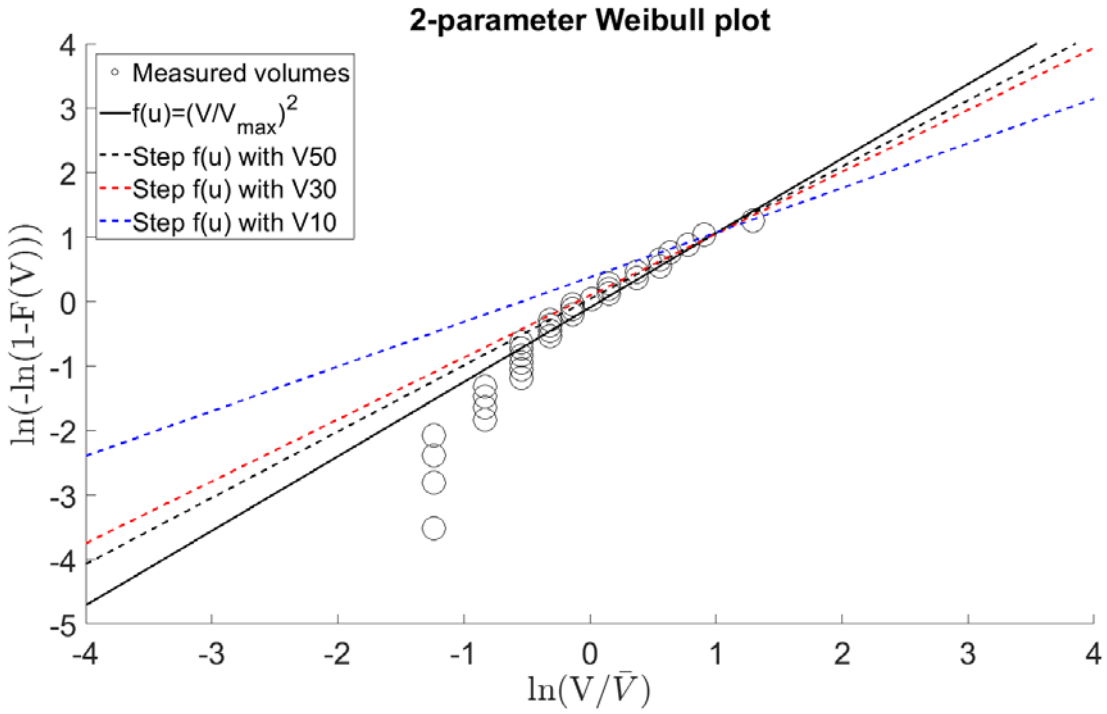

Figure 7. Measured and estimated individual wave overtopping volumes corresponding to Test #32 with P_{ow}=0.033 using the quadratic utility function f(u)=$(V/V_{max})^2$ and the step utility functions with V10, V30 and V50.

The Mean Squared Error (MSE) and the relative Mean Squared Error (rMSE) given by Eqs. (24) and (25), respectively, are used in this study to measure the goodness of fit between estimated and measured data. rMSE measures the proportion of variance in the observations "o" not explained by the estimator "e". The lower the rMSE, the better.

$$MSE = \frac{\sum_{i=1}^{N} \left(Ye_i - Yo_i\right)^2}{N} \tag{24}$$

$$rMSE = \frac{MSE}{Var(Yo)} \tag{25}$$

where "*e*" refers to the estimator; Y*e* and Y*o* are the estimated and observed values, respectively; *N* is the total number of data, and *i* is the data index (i=1,2,….,N).

6. Number of overtopping waves, N_{ow}.

6.1Estimated N_{ow} with methods given in the literature

In this section the performance of the formulas to estimate N_{ow} given in Section 2 are analyzed. Most of the existing formulas are not valid for low $P_{ow}= N_{ow}/N_w$; however, they were applied here to obtain information about its performance with low P_{ow}, which is the common case in conventional mound breakwaters protecting harbors. In the following analysis, N_{ow} is the number of overtopping waves measured value in a given test.

Figure 8 compares the measured and estimated N_{ow} using different estimators valid for conventional mound breakwaters. In this study, $R_c>A_c$, and Eq. (15) was not applicable. Eq. (12) given by Besley [8] and Eq. (16) given by EurOtop [2] were used with γ_f [cube, 2-layer]=0.50, γ_f [Cubipod, 1-layer]=0.46 and γ_f [Cubipod, 2-layer]=0.44 proposed by Smolka et al. [20]. Eq. (12) given by Besley [8] was used with K1=50.8 for the armor slope cotα =1.5, interpolated from values given for armor slopes cotα =2 and cotα =1.

Eq. (12) and Eq. (16) provided poor N_{ow} (N_w=1000) predictions while Eq. (13) given by Besley [8] and Eq. (14) given by Nørgaard et al. [12] agreed quite well with experimental data in this study. However, Eqs. (13) and (14) underpredicted N_{ow} if measured $N_{ow}>30$ and overpredicted N_{ow} if measured $N_{ow}<10$. The rMSE on all data of Eqs. (13) and (14) in Figure 8 are rMSE=11.3% and 11.9%, respectively. According to Eq. (10), the larger the N_{ow}, the larger the V_{max}; a new estimator is developed in Section 7 to better calculate the number of overtopping waves (N_{ow}).

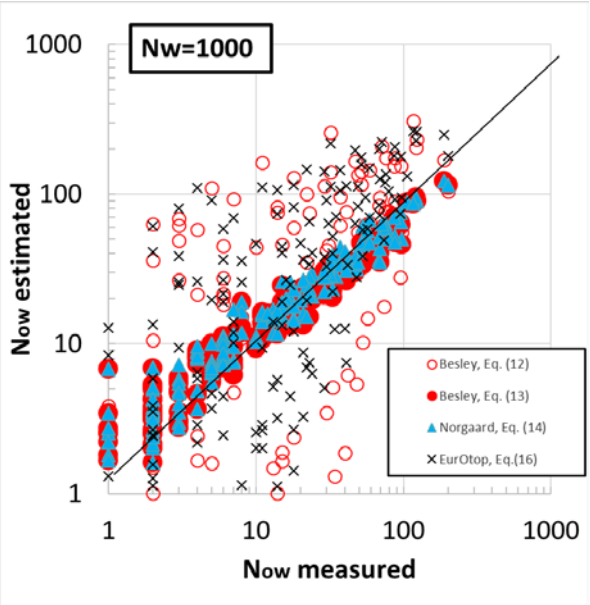

Figure 8. Comparison between measured and estimated N_{ow}.

6.2 *A new method to estimate N_{ow}*

In this study, the parameters G_1 and G_2 in $P_{ow}=G_1\ Q^{*G2}$, similar to Eq. (13a), were calibrated minimizing MSE of $\ln(N_{ow})$. Figure 9 illustrates the goodness of fit of Eq. (26) with rMSE=6.7%.

$$P_{ow} = \frac{N_{ow}}{N_w} = 480Q^{*0.8} \tag{26}$$

where $Q^*= q/(gT_{01}H_s)$ is the dimensionless mean overtopping discharge, P_{ow} is the proportion of overtopping waves, N_w is the number of waves and N_{ow} is the number of overtopping events. In this study, the variance was not considered as constant as in Herrera and Medina [23]. Thus, following the methodology given by Herrera and Medina [23], the error (ε) may be considered as Gaussian distributed with 0 mean and variance estimated by:

$$\sigma^2(\varepsilon) = -0.042 ln N_{ow} + 0.23 \tag{27}$$

The 5% and 95% percentiles for the N_{ow} estimations given by Eq. (26) may be obtained by:

$$lnN_{ow}|_{5\%}^{95\%} = lnN_{ow} \pm 1.65\sqrt{-0.042lnN_{ow} + 0.23} \quad (28)$$

The range of application of Eq. (26) is $0.001 \leq P_{ow} < 0.200$ and $7.0 \cdot 10^{-8} \leq Q^* \leq 6.4 \cdot 10^{-5}$, in the lowest part of the range of application of Eq. (13a).

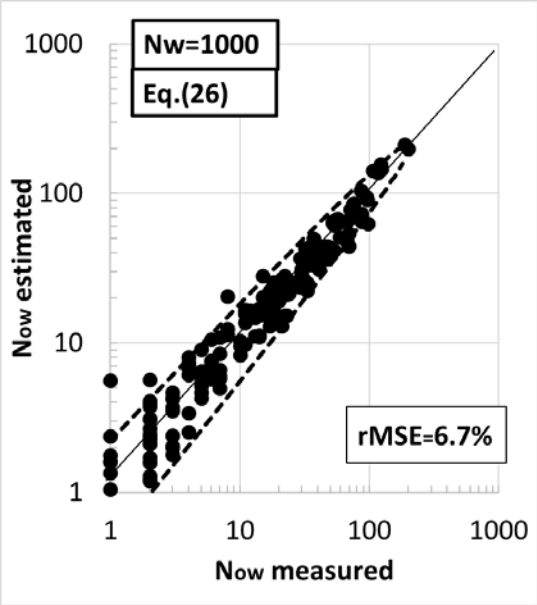

Figure 9. Comparison between N_{ow} measured and estimated by Eq. (26) and 90% confidence interval.

7. Maximum individual wave overtopping volume, V_{max}.

7.1 Estimated V_{max} with methods given in the literature.

In this section the performance of the formulas to estimate V_{max} given in Section 2 is analyzed. Most of the existing formulas are not valid for low $P_{ow} = N_{ow}/N_w$, but they were applied here to obtain information about its performance with low V_{max}, which is the common case in conventional mound breakwaters protecting harbors. In the following analysis, q, N_{ow}, V_{total} and V_{max} are measured values in a given test, q(l/s/m) is the mean overtopping discharge, N_{ow} is the number of overtopping waves, V_{total}(l/m) is the total accumulated overtopped volume and V_{max}(l/m) is the highest individual wave overtopping volume.

Figure 10 compares the measured and estimated dimensional V_{max} and dimensionless $V_{max}^*=V_{max}/(gH_sT_{01}^2)$ using various formulas, valid for conventional mound breakwaters with $\bar{V} = V_{total}/N_{ow}$ where V_{total}(l/m) and N_{ow} are measured values. The scale factor of the Weibull distribution (A) is estimated using Eq. (3) as suggested in the literature. The existing estimators of V_{max}^* underpredicted V_{max}^* if $V_{max}^*<10^{-4}$ or $V_{max}^*>10^{-3}$ with rMSE on all data of 15%<rMSE<22%. The 2-parameter Weibull and Exponential distributions are analyzed in Sections 7 and 8 to better estimate V_{max}^*.

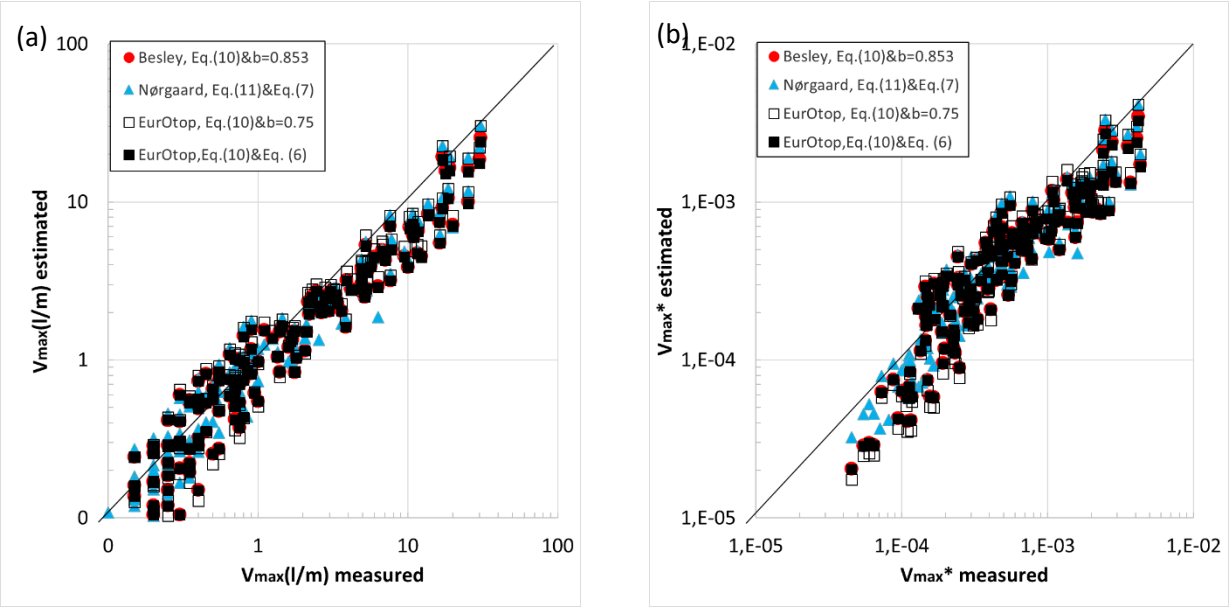

Figure 10. Comparison between measured and estimated (a) V_{max} (l/m) and (b) $V_{max}^*=V_{max}/(gH_sT_{01}^2)$.

7.2 A new method using the Weibull distribution to estimate V_{max}

The maximum individual wave overtopping volume is evaluated using Eq. (10); V_{max} depends on N_{ow}, b, A and $\bar{V} = V_{total}/N_{ow}$. The shape and scale factors (b and A) of the Weibull distribution derived from each test are analyzed here depending on the utility function f(u) used to fit them.

Figure 11a illustrates the relationship between Q* and b and the least-squares fitting given by Eq. (29a). Figure 11b illustrates the relationship between 1/b and A and the least-squares fitting given by Eq. (29b).

Figures similar to Figure 11 were obtained using the step utility function with 10%, 30% and 50% of the highest individual wave overtopping volumes. Hereafter, $A[V^2]$ and $b[V^2]$ are the estimated Weibull parameters considering $f(u)=(V/V_{max})^2$; A[V50] and b[V50] are those considering a step utility function with VP=V50; A[V30] and b[V30] are those considering a step utility function with VP=V30 and A[V10] and b[V10] are those considering a step utility function with VP=V10.

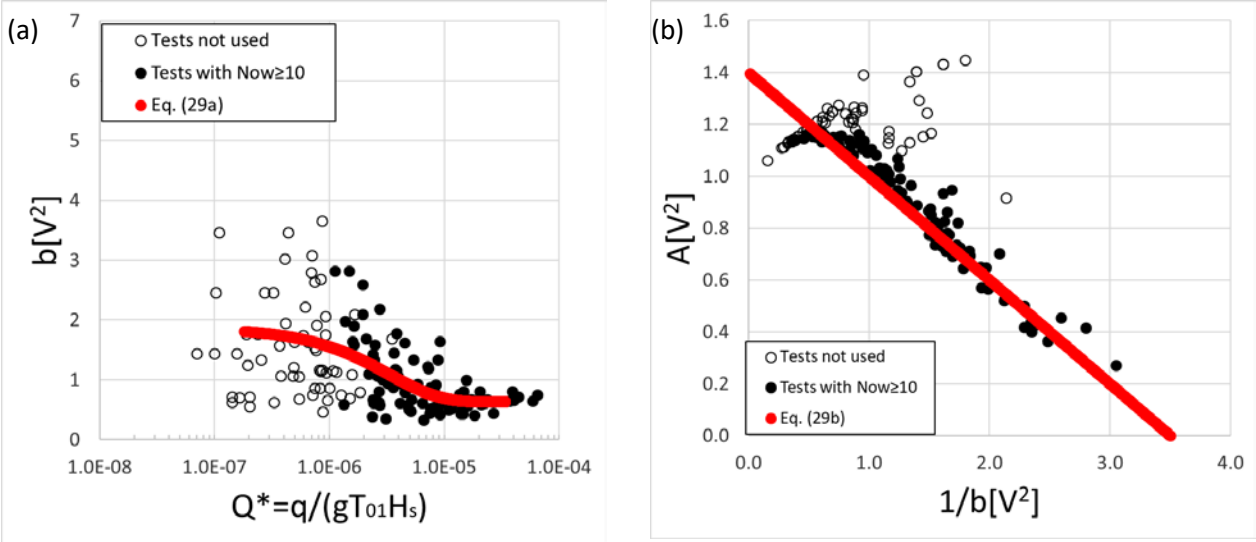

Figure 11. Relationship with explanatory variables and least-squares fitting using $f(u)=V^2$ of (a) Weibull's shape factor, $b[V^2]$, and (b) Weibull's scale factor, $A[V^2]$.

Eqs. (29) to (32) provide the estimation of A and b for the utility functions used in this study:

$$b[V^2] = 0.63 + 1.25\exp(-3.0 \cdot 10^5 Q^*) \quad (29a)$$

$$A[V^2] = 1.4 - 0.4\frac{1}{b[V^2]} \quad (29b)$$

$$b[V50] = 0.58 + \exp(-2.6 \cdot 10^5 Q^*) \quad (30a)$$

$$A[V50] = 1.3 - 0.4\frac{1}{b[V50]} \quad (30b)$$

$$b[V30] = 0.63 + 3.5\exp(-8.5 \cdot 10^5 Q^*) \quad (31a)$$

$$A[V30] = 1.3 - 0.36\frac{1}{b[V30]} \quad (31b)$$

$$b[V10] = 0.79 + 14.5\exp(-1.0 \cdot 10^6 Q^*) \quad (32a)$$

$$A[V10] = 1.3 - ln\left(\frac{1}{b[V10]}\right) \quad (32b)$$

where $Q^* = q/(gT_{01}H_s)$. The range of application for Eqs. (29) to (31) is $0.010 \leq P_{ow} \leq 0.200$ and $1.1 \cdot 10^{-6} \leq Q^* \leq 6.4 \cdot 10^{-5}$ and for Eq. (32) is $0.020 \leq P_{ow} \leq 0.200$ and $2.0 \cdot 10^{-6} \leq Q^* \leq 6.4 \cdot 10^{-5}$.

Regardless of the utility function used, the shape factor (b) depends on the dimensionless wave overtopping discharge $Q^* = q/(gT_{01}H_s)$, and the scale factor (A) depends on 1/b. To avoid inconsistencies in tests with low N_{ow} when using the quadratic utility function and the step utility functions with VP=V30 and VP=V50, only tests with $N_{ow} \geq 10$ ($P_{ow} \geq 0.01$) were considered to fit A and b. When using the step utility function with VP=V10, only tests with $N_{ow} \geq 20$ ($P_{ow} \geq 0.02$) were considered in the analysis.

Figure 12 illustrates the performance of Eq. (10) to estimate $V_{max}^* = V_{max}/(gH_sT_{01}^2)$ with measured N_{ow} and $\bar{V}$ and using Eqs. (29) to (32) to estimate A and b. Figure 12 shows that Eqs. (29) to (31) improve the prediction of V_{max}^* compared to the existing methods (see Figure 10), especially for small and large V_{max}^*. Eq. (29) corresponding to the quadratic utility function provides the lowest rMSE=10.4% on all data. Assuming a Gaussian error distribution with constant variance, the 90% confidence interval of Eq. (29) is given by $lnV_{max}^*|_{5\%}^{95\%} = lnV_{max}^* \pm 0.57$. Eq. (32) with a step utility function with VP=V10 clearly overpredicts V_{max}^* for low values of V_{max}^* associated with P_{ow} <0.01<0.02, beyond the range of application of Eqs. (32).

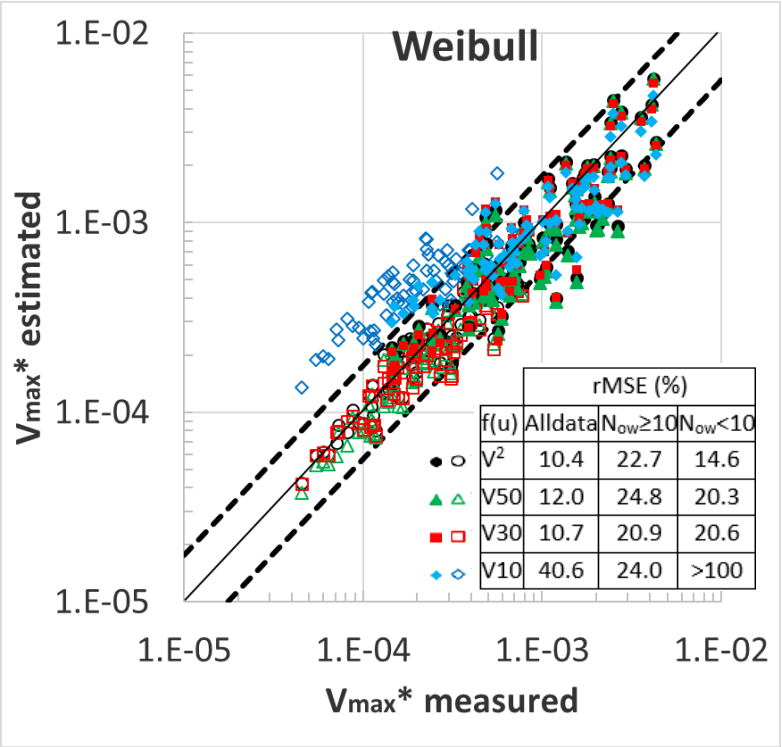

Figure 12. Comparison between measured and estimated V_{max}*= $V_{max}/(gH_sT_{01}^2)$ by the Weibull distribution using different utility functions. 90% confidence interval refers to the quadratic utility function. Solid symbols correspond to data with $0.20>P_{ow}\geq0.01$ and empty symbols correspond to data with $P_{ow}<0.01$.

7.3 A new method using the Exponential distribution to estimate V_{max}

Distributions different from the 2-parameter Weibull one may be used to fit the larger individual wave overtopping volumes; in this study the performance of the 2-parameter Exponential distribution is analyzed. The 2-parameter Exponential distribution is given by Eq. (33), where c and d are the two free parameters.

$$F(V) = 1 - exp\left[-\left(\frac{V-c}{d}\right)\right] \quad (33)$$

Eq. (33) can be rewritten using the dimensionless parameters C= $c/\bar{V}$ and D= $d/\bar{V}$, where $\bar{V}$ is the measured mean individual wave overtopping volume. An Exponential plot can be generated considering logarithms on both sides of Eq. (33).

$$-ln\big(1-F(V)\big)=\frac{V/\bar{V}}{D}-\frac{C}{D} \quad (34)$$

Thus, the Exponential plot can be represented considering $-\ln\big(1-F(V)\big)$ in the y-axis and $V/\bar{V}$ in the x-axis. Like Eq. (10) for the Weibull distribution, the maximum overtopping volume of an Exponential distribution is given by:

$$V_{max}=D\bar{V}[\ln(N_{ow}+1)+C/D] \quad (35)$$

The parameters C and D of the Exponential distribution were calibrated following the same methodology described in Section 7.2:

$$D[V^2]=2.6-2.6\exp(-3.0\cdot10^5Q^*) \quad (36a)$$

$$C[V^2]=1.2-D[V^2]-0.2D[V^2]^2 \quad (36b)$$

$$D[V50]=2.1-2\exp(-3.5\cdot10^5Q^*) \quad (37a)$$

$$C[V50]=1.4-1.4D[V50] \quad (37b)$$

$$D[V30]=2.3-2.5\exp(-4.5\cdot10^5Q^*) \quad (38a)$$

$$C[V30]=1.7-1.7D[V30] \quad (38b)$$

$$D[V10]=2.7-7\exp(-5.0\cdot10^5Q^*) \quad (39a)$$

$$C[V10]=2.8-2.5D[V10] \quad (39b)$$

The range of application for Eqs. (36) to (38) is $0.010 \leq P_{ow} < 0.200$ and $1.1 \cdot 10^{-6} \leq Q^* \leq 6.4 \cdot 10^{-5}$, and for Eq. (39) is $0.020 \leq P_{ow} < 0.200$ and $2.0 \cdot 10^{-6} \leq Q^* \leq 6.4 \cdot 10^{-5}$.

Figure 13 illustrates the performance of Eq. (35) to estimate $V_{max}^* = V_{max}/(gH_sT_{01}^2)$ with measured N_{ow} and $\bar{V}$ and using Eqs. (36) to (39) to estimate the two parameters of the Exponential distribution. Figure 13 shows that Eqs. (36) to (38) improve the prediction of V_{max}^* compared to existing methods (see Figure 10) and provide predictions similar to the 2-parameter Weibull distribution (see Figure 11). Eq. (36) corresponding to the quadratic utility function provides rMSE=10.6% on all data. Assuming a Gaussian error distribution with constant variance, the 90% confidence interval of Eq. (36) is given by $lnV_{max}^*|_{5\%}^{95\%} = lnV_{max}^* \pm 0.57$. Eq. (39) with a step utility function with VP=V10 clearly overpredicts V_{max}^* for low values of V_{max}^* associated with $P_{ow} < 0.01 < 0.02$, beyond the range of application of Eqs. (39).

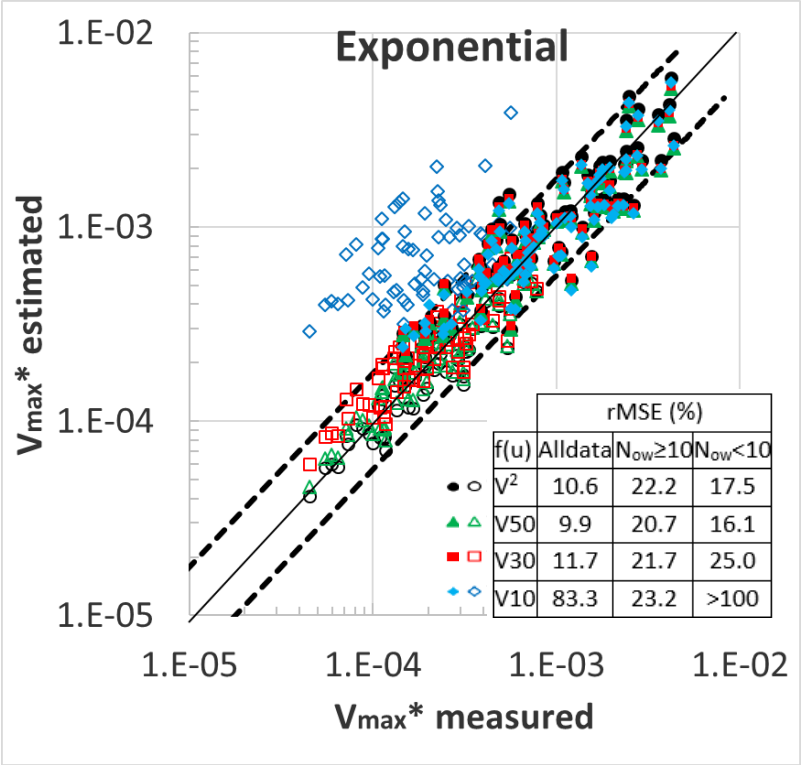

Figure 13. Comparison between measured and estimated $V_{max}^* = V_{max}/(gH_sT_{01}^2)$ by the Exponential distribution using different utility functions. 90% confidence interval refers to the quadratic utility

function. Solid symbols correspond to data with $0.20>P_{ow}\geq0.01$ and empty symbols correspond to data with $P_{ow}<0.01$.

7.4 Estimation of N_{ow} and V_{max} using the CLASH Neural Network

During the design stage, the geometry of the breakwater and the design storm (H_s and T_{01}) are given. Thus, q and N_{ow} can be estimated with formulas given in the literature, and $\bar{V}$ can be calculated as $\bar{V} = qT_{01}N_w/N_{ow}$. In this section, the CLASH Neural Network (see Van Gent et al. [3] and CLASH [24]) is used to estimate q with the roughness factors proposed by Molines and Medina [5]; N_{ow} is estimated using Eq. (26), and V_{max} is estimated by Eq. (10) using the Weibull parameters (A and b) -given by Eq. (29), and Eq. (35) with the Exponential parameters (C and D) given by Eq. (36).

Figure 14a illustrates the goodness of fit of the CLASH Neural Network to estimate Q* with rMSE=30% and Figure 14b illustrates the goodness of fit of Eq. (26) to estimate N_{ow} with rMSE=31%.

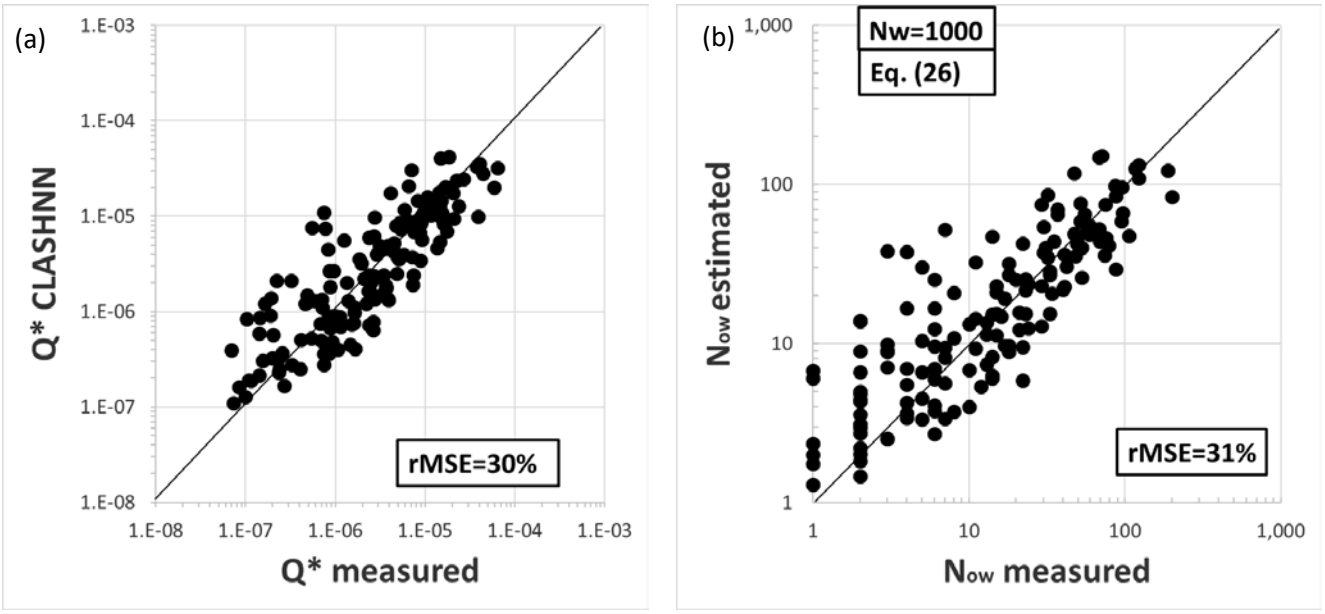

Figure 14. Comparison between measured and estimated values of (a) Q* using the CLASH Neural Network and (b) N_{ow} using Eq. (26).

Figure 15 illustrates the performance of Eqs. (10) and (35) to estimate V_{max} based on estimated N_{ow} and $\bar{V}$. Eqs. (29) and (36) were used to estimate the Weibull and Exponential parameters associated to the quadratic utility function, respectively. V_{max}* estimated by the Weibull and Exponential distributions show rMSE=31.6% and 33.3%, respectively. Using estimated values of q and P_{ow}, Figure 15 shows that the prediction error of V_{max}* is higher than that using measured q and measured $\bar{V}$.

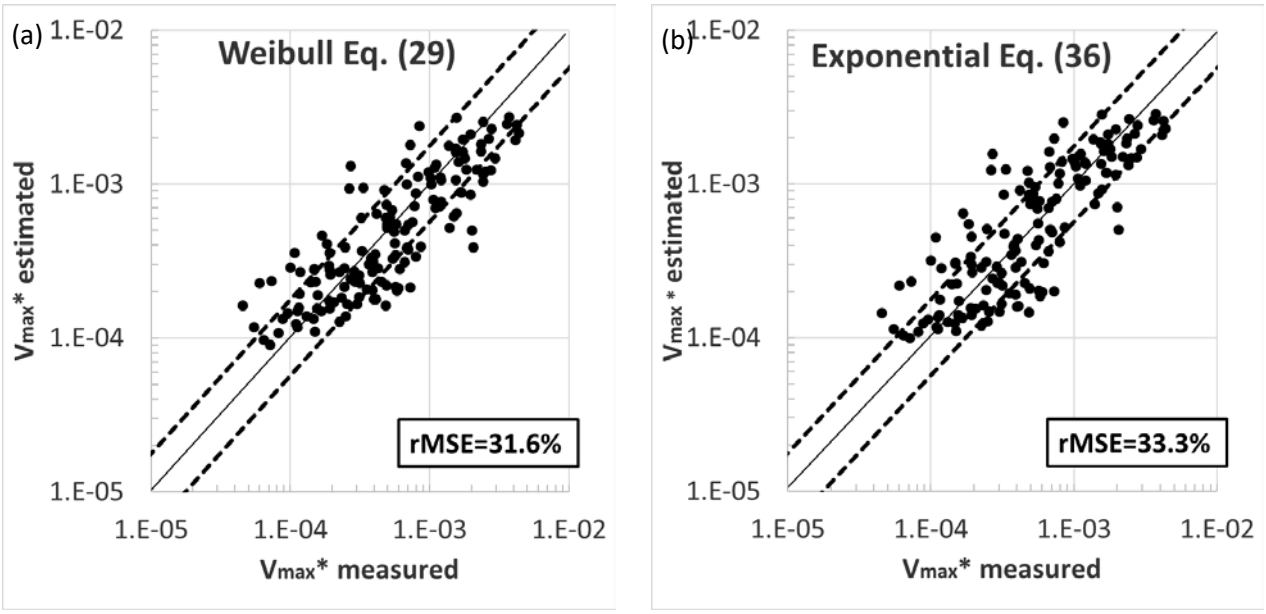

Figure 15. Comparison between measured and estimated V_{max}*= $V_{max}/(gH_sT_{01}^2)$ with 90% confidence intervals using the mean wave overtopping rate (q) predicted by the CLASH Neural Network and (a) Weibull distribution and (b) Exponential distribution.

8. Conclusions

Conventional mound breakwaters are usually designed with a crest freeboard level that allows low mean wave overtopping discharges (q), low maximum individual wave overtopping volumes (V_{max}) and a low proportion of overtopping waves ($P_{ow}=N_{ow}/N_w$). Existing formulas to estimate P_{ow} are usually based on tests with large P_{ow}; this study is focused on mound breakwaters with low N_{ow} (P_{ow} < 0.2). This research analyzes the performance of the Weibull and Exponential distributions to estimate the individual wave

overtopping volumes. To this end, a new methodology was developed to identify the N_{ow} and the individual wave overtopping volumes based on a continuous record of accumulated overtopping volumes in 2D physical tests. The methodology was applied to 164 small-scale 2D tests carried out by Smolka et al. [20] to propose a new estimator for the number of overtopping waves (N_{ow}) and to fit 2-parameter Weibull and Exponential distributions for individual wave overtopping volumes, F(V). A quadratic utility function $f(u)=(V/V_{max})^2$, using all the data, and a step utility function using only 10%, 30% and 50% of the highest individual wave overtopping volumes were considered to fit the 2-parameter Weibull and Exponential distributions.

When compared to experimental observations, Eqs. (13) and (14) given by Besley [8] and Nørgaard et al. [12] were the best estimators of N_{ow}, yet both formulas underpredicted N_{ow} if $N_{ow}>30$ and overpredicted N_{ow} if $N_{ow}<10$. In this study, a new estimator of N_{ow} given by Eqs. (26) and (28) is proposed with rMSE=6.7%.

In the literature, the scale factor (A) of the Weibull distribution is usually related to the shape factor (b) using the measured mean individual wave overtopping volume, $\bar{V}$. However, $\bar{V}$ considers low individual wave overtopping volumes, which are not easily measured during laboratory tests and are not relevant for most practical applications. Estimators given by Besley [8], EurOtop [1, 2] and Nørgaard et al. [12] underpredicted the observed $V_{max}^*= V_{max}/(gH_sT_{01}^2)$ if $V_{max}^*<10^{-4}$ or $V_{max}^*>10^{-3}$. The new 2-parameter Weibull and Exponential distributions provide unbiased estimations of V_{max}^* with rMSE=10.4% and 10.6%, respectively, when using the quadratic utility function.

The 2-parameter Weibull and Exponential distributions may be used to estimate the larger individual wave overtopping volumes. Eqs. (29) to (31) and (36) to (38) can be used to estimate the parameters of the distributions; predictions for V_{max}^* using those parameters gave good agreements except the parameters fitted to the top highest 10% individual wave overtopping volumes, which provided

unreliable overestimations for both the Weibull and Exponential distributions when P_{ow}<0.01. The use of the highest 10% of volumes to fit the Weibull or Exponential distribution is only relevant when N_{ow} is sufficiently large. Using a low N_{ow} to fit the statistical distribution (e.g. the highest 10% overtopping waves) might lead to poor predictions.

When measured q and N_{ow} are not available, coastal engineers can estimate these variables using formulas given in the literature. The CLASH Neural Network was used in this study to estimate q on the 164 small-scale tests. Using the new estimator for N_{ow} given by Eq. (26) with q predicted by the CLASH Neural Network, estimations of N_{ow} have rMSE=31%. Using the quadratic utility function and the estimated q and N_{ow}, V_{max}* was calculated by the Weibull and Exponential distributions with rMSE=31.6% and 33.3%, respectively. Using estimated q and $P_{ow}=N_{ow}/N_w$, the prediction error of V_{max}* is higher than that using measured q and measured $\bar{V}$ due to the estimation error of q.

Acknowledgments

The authors are grateful for financial support from European FEDER and Spanish *Ministerio de Economía y Competitividad* (Grants BIA2012-33967 and BIA2015-70435-R), SATO (OHL Group), *Universitat Politècnica de València* (Grant SP20180111, *Primeros Proyectos de Investigación (PAID-06-18), Vicerrectorado de Investigación, Innovación y Transferencia de la Universitat Politècnica de València)* and CDTI (*Centro para el Desarrollo Tecnológico e Industrial*). The authors also thank Debra Westall for revising the manuscript.

References

[1] EurOtop, 2007. Wave Overtopping of Sea Defences and Related Structures: Assessment Manual (EurOtop Manual). Pullen, T., Allsop, N.W.H., Bruce, T., Kortenhaus, A., Schüttrumpf, H., Van der

Meer, J.W. Environment Agency, UK/ENW Expertise Netwerk Waterkeren, NL/KFKI Kuratorium für Forschung im Küsteningenieurwesen, Germany, 193 p.

[2] EurOtop, 2018. Manual on wave overtopping of sea defences and related structures. An overtopping manual largely based on European research, but for worldwide application. Van der Meer, J.W., Allsop, N.W.H., Bruce, T., De Rouck, J., Kortenhaus, A., Pullen, T., Schüttrumpf, H., Troch, P., Zanuttigh, B., www.overtopping-manual.com. (Accessed: 12th February 2019).

[3] Van Gent, M.R.A., Van den Boogaard, H.F.P., Pozueta, B., Medina, J.R., 2007. Neural network modelling of wave overtopping at coastal structures. Coastal Engineering, 54 (8), 586–593.

[4] Molines, J., Medina, J.R., 2015a. Explicit wave overtopping formula for mound breakwaters with crown walls using CLASH neural network derived-data. Journal of waterway, Port, Coastal and Ocean Engineering, 142 (3), 10.1061/(ASCE)WW.1943-5460.0000322, 04015024.

[5] Molines, J., Medina, J.R., 2015b. Calibration of overtopping roughness factors for concrete armor units in non-breaking conditions using the CLASH database. Coastal Engineering, 96, 65-70.

[6] Franco, L., de Gerloni, M., van der Meer, J.W., 1994. Wave overtopping on vertical and composite breakwaters. Proc. 24th International Conference on Coastal Engineering, ASCE, pp. 1030–1044.

[7] Van der Meer, J.W., Janssen, J.P.F.M., 1994. Wave Run-Up and Wave Overtopping at Dikes, Delft Hydraulics No. 485, 22 p.

[8] Besley, P., 1999. Overtopping of sea-walls-design and assessment manual. R & D Technical Report 178, Environment Agency, Bristol, UK.

[9] Lykke-Andersen, T., Burcharth, H. F., Gironella, F. X., 2009. Single wave overtopping volumes and their travel distance for rubble mound breakwaters. Coastal Structures 2007: Proc. of the 5th International Conference, World Scientific, pp. 1241-1252.

[10] Victor, L., van der Meer, J.W., Troch, P., 2012. Probability distribution of individual wave overtopping volumes for smooth impermeable steep slopes with low crest freeboards. Coastal Engineering, 64, 87-101.

[11] Zanuttigh, B., van der Meer, J.W., Bruce, T., Hughes, S., 2013. Statistical characterization of extreme overtopping wave volumes. Proc. of the ICE, Coasts, Marine Structures and Breakwaters, ICE Publishing (London, UK), Vol. 1, pp. 442-452.

[12] Nørgaard, J.Q.H., Lykke-Andersen, T., Burcharth, H.F., 2014. Distribution of individual wava overtopping volumes in shallow water wave conditions. Coastal Engineering, 83, 15-23.

[13] Pan, Y., Lin, L., Amini, F., Kuang, C., Chen, Y., 2016. New understanding on the distribution of individual wave overtopping volumes over a levee under negative freeboard. Journal of Coastal Research, 75, 1207-1211.

[14] Gallach, D., 2018. Experimental study of wave overtopping performance of steep low-crested structures. PhD Thesis, Ghent University, 182 p.

[15] Hughes, S.A., Thornton, C., van der Meer, J., Scholl, B., 2012. Improvements in describing wave overtopping processes. Proc. 33th International Conference on Coastal Engineering, ASCE, pp. 2085–2009.

[16] Franco, C., 1996. Wave Overtopping and Loads on Caisson Breakwaters under Three Dimensional Sea States, DelfttHydraulics.

[17] Bruce, T., van der Meer, J.W., Franco, L., Pearson, J.M., 2009. Overtopping performance of different armour units for rubble mound breakwaters. Coastal Engineering, 56, 166-179.

[18] Hughes, S.A., Nadal, N.C., 2009. Laboratory study of combined wave overtopping and storm surge overflow of a levee. Coastal Engineering, 56(3), 244-259.

[19] Makkonen, L., 2006. Plotting positions in extreme values analysis. Journal of Applied Meteorology and Climatology, 45, 334-340.

[20] Smolka, E., Zarranz, G., Medina, J.R., 2009. Estudio Experimental del Rebase de un Dique en Talud de Cubípodos. Libro de las X Jornadas Españolas de Costas y Puertos, Universidad de Cantabria-Adif Congresos, pp. 803-809 (in Spanish).

[21] Molines, J., Herrera, M.P., Medina, J.R., 2018. Estimations of wave forces on crown walls based on wave overtopping rates. Coastal Engineering, 132, 50-62.

[22] Figueres, M., Medina, J.R., 2004. Estimating incident and reflected waves using a fully nonlinear wave model. Proc. 29th International Conference on Coastal Engineering, World Sicentific, pp. 594-603.

[23] Herrera, M.P., Medina, J.R., 2015. Toe berm design for very shallow waters on steep sea bottoms. Coastal Engineering, 103, 67-77.

[24] Crest Level Assessment of coastal Structures by full scale monitoring, neural network prediction and Hazard analysis on permissible wave overtopping, 2001-2003, http://www.clash.ugent.be/ (Accessed: 7th November 2018).